Journal of Science and Technology in Civil Engineering, HUCE, 2025, 19 (4): 18–28

EFFECT OF PARTICLE DENSITY ON POWDER MIXING IN NUCLEAR FUEL PELLET FABRICATION USING DISCRETE ELEMENT METHOD

Duc Chung Vu[a,*], Farhang Radjai[b]

[a]*Faculty of Hydraulic Engineering, Hanoi University of Civil Engineering, 55 Giai Phong road, Bach Mai ward, Hanoi, Vietnam*
[b]*University of Montpellier, CNRS, LMGC, 163 rue Auguste Broussonnet, Montpellier, 34090, France*

Article history:
Received 21/5/2025, Revised 21/8/2025, Accepted 12/9/2025

Abstract

Granular mixing is a fundamental operation in the fabrication of mixed-oxide (MOX) nuclear fuels, where achieving homogeneous blends of constituent materials is essential for reactor performance and safety. Using particle dynamics simulations, we investigate the flow behavior and binary mixing of equi-sized spherical particles with differing densities in horizontal rotating drums operating within the cascading regime. An extensive parametric study is conducted by systematically varying the particle density while keeping all other particle properties fixed. The simulation results indicate that mixtures composed of particles with similar densities undergo efficient mixing, whereas mixtures with large density contrasts exhibit persistent segregation. In the latter case, denser particles are concentrated near the drum core, while lighter particles settle away from the core. Additionally, the curvature of the free surface is observed to increase monotonically with the particle density ratio, indicating a strong coupling between density-driven segregation and surface flow dynamics. These findings provide insights into the mechanisms governing density segregation in rotating drums and have implications for optimizing mixing processes in industrial and nuclear fuel fabrications contexts.

Keywords: binary mixing; equi-sized spherical particles; segregation; fuel pellet; nuclear reactor; discrete element method.

https://doi.org/10.31814/stce.huce2025-19(4)-02

1. Introduction

In the field of nuclear energy, minimizing the amount of waste products from nuclear power plants is one of the challenges for scientists [1–4]. Closed fuel cycles have been developed to recycle the waste products into new fuel. A closed fuel cycle begins with the fabrication of uranium oxide (UOX) pellets which is used in nuclear reactors. After UOX has been used, it is removed and sent to a reprocessing plant where the uranium and plutonium are separated from spent fuel. The uranium is then recycled into new fuel pellets, while the plutonium is used to produce mixed oxide (MOX) fuel. MOX fuel is a mixture of uranium and plutonium oxide, and it can be used in place of conventional UOX fuel in nuclear reactors [1, 2, 5, 6].

MOX pellets are manufactured by powder metallurgy, but the flow-sheet is more complex because there are two different powders that need to be mixed [3, 6, 7]. Due to moderate diffusion coefficients of uranium and plutonium at high temperatures, simply mixing uranium oxide and plutonium oxide powders is insufficient to achieve a very homogeneous uranium-plutonium spatial distribution, thus improving the fuel characteristics [8–11]. Indeed, a large concentration of plutonium can lead to the typical high burn up structure. The first stage of fabrication is therefore a simultaneous milling of

*Corresponding author. *E-mail address:* chungvd@huce.edu.vn (Vu, D. C.)

both powders in the rotating drum with low alloy uranium balls. This operation is performed during several hours, the agglomerates are reduced in size and a thorough mixing of the two powder is achieved [3, 12].

To improve the performance of the mixed powders while minimizing the energy cost, the mixing process in rotating drums is a major subject of current research. Depending on the operation conditions, six flow regimes have been identified for describing the powder motion in a rotating drum: slipping, slumping, rolling, cascading, cataracting and centrifuging [13–15]. The cascading regime has been extensively used in the industrial applications since it accelerates the convection, mixing, segregation, and milling process of the powders [14, 16–18]. However, the cascading regime has received much less attention and has been only recently studied on a systematic basis [17, 19]. This is due to the complex of cascading regime compared to other regimes such as rolling regime where the inertial effects govern the flow behaviour. In cascading regime, both centrifugal force and inertial force control the motion of particles. The particles cascade downward due to gravity, the free surface of flow is curved, and the flow is decomposed in two distinct layers, namely active and passive layer [20, 21].

Previous experimental and numerical studies have indicated that the efficiency of particle mixing and segregation in a rotating drum is a function of certain variables such as particle shape and size, particle density, rotation speed, filling degree, and friction coefficient [22–25]. For instance, the binary mixing of spheres and ellipsoids was studied and it was found that the ellipsoids were segregated to the core of granular bed [26, 27]. The segregation of a binary mixture of differing density (but same size) granular material in rolling regime varies as a function of two fundamental quantities: density ratio of particles and rotation speed of the drum [28]. However, the effects of particle density on the mixing process in the cascading regime have rarely been discussed.

In this paper, we use discrete element method (DEM) simulations to analyze the binary mixture in cascading regime of equal-sized spherical particles and vary the density ratio between two species. The periodic boundary conditions are imposed along the drum axis to eliminate the end wall effects. This makes the flow invariant along the drum axis. The time dependence of the mixing process and the influences of the density ratio on the mixing index are studied. Moreover, we also analyze flow variables such as the average and maximum slopes of the free surface, flow thickness, and velocity field as a function of the particle density ratio.

The paper is structured as follows: In Section 2, we introduce the numerical procedures used in the present study. The mixing process is analyzed in Section 3. The influences of particle density ratio on the drum flow variables are investigated in Section 4. Finally, we summarize and discuss the key findings of this study in Section 5.

2. Numerical model and procedures

2.1. Method description

DEM is a powerful and reliable research tool. This method is based on the integration of equations of motion (translations and rotations) for all particles, described as rigid elements, by considering contact forces and external forces acting on the particles. In DEM, the equations of motion are discretized in time and only the rigid-body displacements are considered. Small overlaps between the particles are allowed and used as strain variable. At each contact point, the normal and tangential forces are expressed as a function of the overlaps and tangential displacements. In this study, we use an open source DEM code called Rockable originally created at CNRS in France to solve the equations of motion [29].

The total interaction force $\vec{f}$ at a contact point between two spherical particles is the sum of the normal and tangential components f_n and f_t, respectively. At each contact point, a linear elastic law which is equivalent to a linear unilateral spring acting the contact point is implemented. To incorporate contact inelasticity, a viscous damping term is added to the normal elastic repulsion force. Let $\vec{n}$ and $\vec{t}$ denote the normal and tangential unit vectors at a contact point c between particles i and j. The contact force $\vec{f} = f_n\vec{n} + f_t\vec{t}$ exerted by particle j on particle i is expressed as a function of the normal overlap h and the cumulative tangential displacement $\vec{\delta}_t$.

The normal force law is defined as follows [30, 31]:

$$f_n = \begin{cases} 0, & \tilde{f}_n \leq 0 \\ \tilde{f}_n, & \tilde{f}_n > 0 \end{cases} \tag{1}$$

where $\tilde{f}_n = k_n h - 2a\sqrt{k_n m}\dot{\delta}_n$, k_n is the normal stiffness, h represents the normal overlap (with $h > 0$ indicating particle overlap), $\dot{\delta}_n$ is the relative normal velocity, m is the reduced mass of the two contacting particles, and a is a dimensionless damping parameter ranging from 0 (fully elastic contact) to 1 (fully inelastic contact). In binary collisions, the normal restitution coefficient decreases as a increases [32, 33]. In DEM simulations, low-frequency vibration modes tend to decay slowly. To counteract this, it is common practice to enhance contact dissipation by setting the restitution coefficient close to zero (i.e., a near 1). In our simulations, we adopted a restitution coefficient of 0.001 to ensure efficient damping.

The tangential force f_t follows the Coulomb friction law:

$$f_t = \min\{|k_t\vec{\delta}_t|,\ \mu_s f_n\} \tag{2}$$

where k_t is the tangential stiffness, δ_t is the cumulative tangential displacement, and μ_s is the inter-particle friction coefficient. The tangential force direction $\vec{t}$ is determined by the relative motion at the contact: it opposes the relative elastic displacement $\vec{\delta}_t$ when below the Coulomb threshold, and the relative tangential velocity $\vec{v}_t$ when the threshold is reached. The graphical representation of the normal and tangential force is shown in Fig. 1.

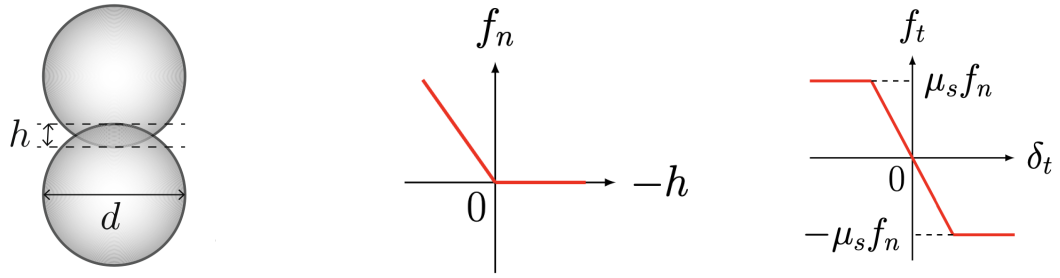

(a) Interaction between two particles with diameter d and overlap h

(b) Graphical representation of the elastic normal force law

(c) Tangential elasto-frictional force law

Figure 1. Graphical representation of the contact geometry and force law between touching particles

2.2. *Sample setup and boundary conditions*

In order to prepare the samples, a drum is created by writing a STL file in Blender which is an open-source software. Then, spherical particles are deposited into the drum until the filling degree reaches the desired value. We consider horizontal drums of diameter $D = 2R$ and width W filled with

monodisperse spheres of diameter d and subjected to a constant rotation speed ω, see Fig. 2. There are two species of spheres: orange and black with different values of particle density. The orange spheres are denser than the black spheres, and the density ratio ρ_o/ρ_b is varied from 1 to 4. The orange and black particles are initially segregated at the side-side loading arrangement as shown in Fig. 2(a). The number of orange and black particles is approximately equal. The filling degree is defined by the ratio $J = h_0/D$, where h_0 is the thickness of the granular flow at the midpoint if the free surface at rest. Periodic boundary conditions are imposed along the drum axis so that the flow is invariant along the width axis. The friction coefficients between particles and with drum wall are set to $\mu_s = 0.4$, which is a common value for smooth drum wall [17].

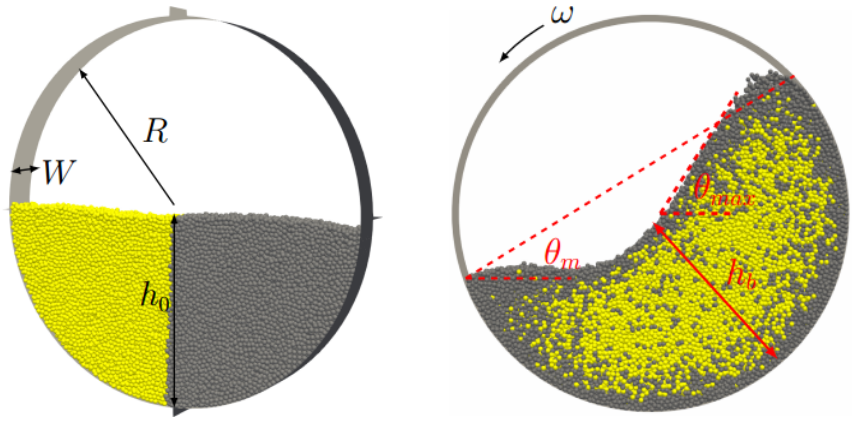

(a) In the initial state (b) In the steady state

Figure 2. Geometrical parameters of granular flow in a rotating drum

Table 1. Simulation parameters

Parameter	Symbol	Value	Unit
Number of particles	N_p	25000	-
Particle density ratio	ρ_o/ρ_b	[1; 4]	-
Normal stiffness	k_n	10^8	N/m
Tangential stiffness	k_t	8×10^7	N/m
Restitution coefficient	e_n	0.001	-
Friction coefficient	μ	0.4	-
Gravity acceleration	g	9.81	m/s^2
Particle diameter	d	0.5	mm
Rotation speed	ω	10	rad/s
Drum diameter	D	82	mm
Drum width	W	8	mm
Filling degree	J	0.49	-

The simulations were carried out for values of ω, D, d, and J as shown in Table 1. As we shall see, with the selected ranges of these parameters, the flow is in cascading regime, which is characterized by a S-shaped free surface. In the Ref. [21], we have proposed a scaling parameter, $\Gamma = \mathrm{Fr}^{0.5}(D/d)^{0.5}J^{0.25}$, where Fr is the Froude number, $\mathrm{Fr} = \omega^2 D/2g$. In combination with the data from Ref. [17], we saw that the cascading regime is observed with Γ varying from 2 to 7 for spherical

particles. Therefore, the values of particle size d, drum size D, filling degree J and rotation speed ω chosen in Table 1 lead to the scaling parameter $\Gamma = 6.84$ ensuring the particle flow in the rotating drum is cascading regime. All simulations were run for at least 8 drum rotations to allow the system to reach the steady sate. The data analyzed in this paper, such as free surface, flow thickness, relative particle velocity are averaged over time in the steady state.

3. Mixing behaviour of granular bed

In this work, the mixing quality is quantified by Lacey's mixing index, M, which has been widely used in rotating drums [27, 34, 35]. The mixing index can be calculated as

$$M = \frac{S_0^2 - S^2}{S_0^2 - S_r^2} \tag{3}$$

where S^2 is the actual mixed-variance of binary particles. S_0^2 is the variance corresponding to the completely separated state and expressed as

$$S_0^2 = p(1-p) \tag{4}$$

where p is the volume ratio of one type of particles in the system. S_r^2 corresponds to the completely mixed state and expressed as

$$S_r^2 = p(1-p)/N_p \tag{5}$$

where N_p is the number of particles in the drum. Note that the above equations are only applicable to systems containing mono-size particles as in this study.

In order to obtain the Lacey's index, the three-dimensional drum should be first divided into finite cells. The drum is separated into a number of cubes with a fixed cell size ($D_s \times W/2 \times D_s$), where $D_s = R/40$, as shown in Fig. 3. Then, the position of the particle center is used to determine which cell the particle is in. Considering that there are no particles in the upper part of the drum, a weighting scheme is used to calculate the mixing index [35]. Therefore, a cell containing a larger number of particles corresponds to a larger weight, while a cell containing a smaller number of particles corresponds to a smaller weight. If there is no particles in a cell, the corresponding weight is 0. Moreover, the variance S^2 of the current mixed state based on the weighting concept is obtained by

$$S^2 = \frac{1}{k}\sum_{i=1}^{N_c} k_i(a_i - \bar{a})^2 \tag{6}$$

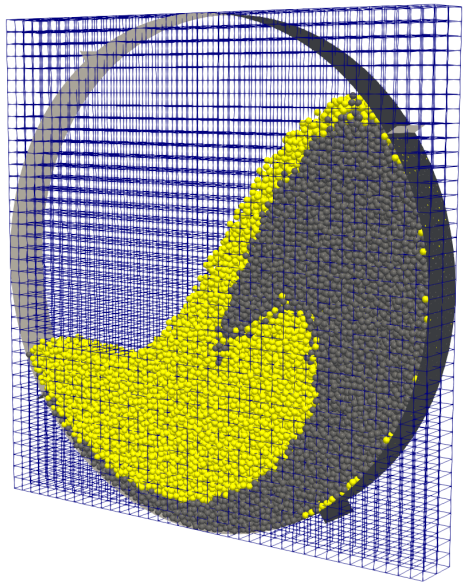

Figure 3. Snapshot of cubic cells in the drum using for calculating the Lacey's mixing index. The cell size is $R/40 \times W/2 \times R/40$

where N_c is the total number of cells in the drum, a_i is the volume ratio of particles of the reference type in a cell, $\bar{a}$ is the volume ratio of particles of the reference type in the drum, and k is the sum of

the weights of all cells, expressed as follows

$$k = \sum_{i=1}^{N_c} k_i \tag{7}$$

where k_i is the weight of cell i, obtained by $k_i = N_i/N_t$, N_i is the number of particles in cell i, and N_t is the total number of particles in all cells. The Lacey's mixing index calculated by Eq. (3) can vary from 0 for completed separation to 1 for total mixing.

Fig. 4 shows the temporal evolution of Lacey's mixing index as a function of the drum rotation number N. The initial value of mixing index is zero, since the orange and black particles are initially segregated at the side-side arrangement. Then, the mixing index gradually increases to reach a residual value which is equal to 0.9 in the case of the same particle densities ($\rho_o/\rho_b = 1$), and much smaller ($\simeq 0.2$) for much different particle densities ($\rho_o/\rho_b = 4$). This means that the mixture with similar particle densities shows better mixing whereas the mixture with different densities shows poor mixing. Moreover, the mixing index increases faster to the constant value in the case of the different densities. For instance, for $\rho_o/\rho_b = 4$ the mixing index is unchangeable after 4 rotations, while for the case of $\rho_o/\rho_b = 1$ the residual value is reached after 7 rotations. The particle density ratio has a strong impact to the binary mixing behavior in the cascading regime which is similar to the rolling regime [36, 37]. However, due to higher particle mobility in cascading regime, the mixing index in steady state is bigger than those of the rolling regime. For example, in the case of $\rho_o/\rho_b = 1$ and the filling degree $J = 0.49$, the mixing index $M = 0.9$ in this study which is bigger than $M = 0.65$ in the Ref. [38].

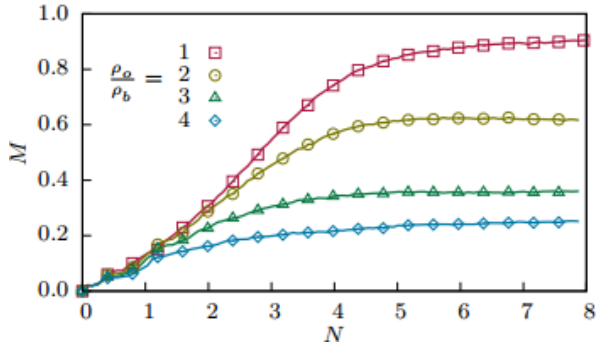

Figure 4. Evolution of the Lacey's mixing index versus drum rotation number N for different values of particle density ratio ρ_o/ρ_b. For clarity, only a selection of data points is displayed.

The evolution of mixing flow patterns for different values of the particle density ratio is displayed in Fig. 5. As the drum rotates, orange/black particles cascade down on the free surface and then enter the passive layer, where the particles are going up, and move as a bulk with the rotating drum wall. Eventually, the particles in the passive layer will mix into the flow layer at the head of the bed surface. As this process repeats constantly, the spiral structure of orange/black color develops as shown in Fig. 5 at the rotation number $N = 2$. Similar spiral structures were also observed from previous simulations for spherical and non-spherical particles [39–41].

Generally, the growth of spiral structures indicates a better mixing quality because of a larger interface between orange and black particles. After 4 rotations the spiral structure disperses significantly for small particle density ratios, but it is concentrated in the case of biggest density ratio. The denser particles (orange) stay around the center of mass of the drum, while the lighter particles (black) are found near the drum wall and free surface. This is due to the larger mass of the denser particles,

when they reach the head, they do not cascade along the top surface. Rather they tend to sink into the bed. As a result, the denser particles are not found in the toe region of free surface, where the mixing process occurs in a rotating drum. That is why the efficiency of mixing is a decreasing function of density ratio.

After sufficient rotations of the drum ($N = 8$), both orange and black particles are able to reach a well-mixed state, where the corresponding mixing index is close to 1, see Fig. 4, in the case of $\rho_o/\rho_b = 1$. The mixing is increasingly inhomogeneous as the particle density ratio increases. Typically the segregation of denser particles occurs quite quickly, within a rotation or two. This system can be therefore used to separate particles in granular materials based on their density.

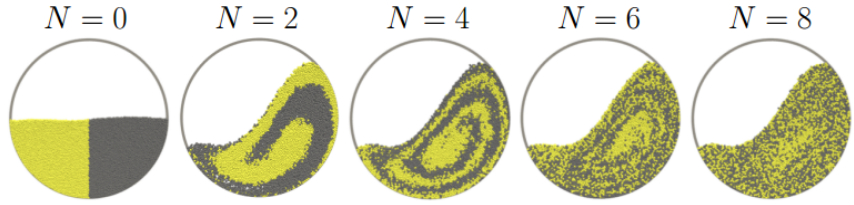

(a) $\rho_o/\rho_b = 1$

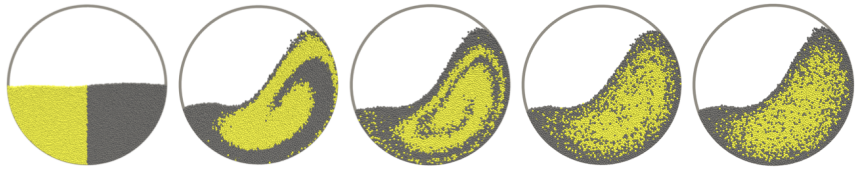

(b) $\rho_o/\rho_b = 2$

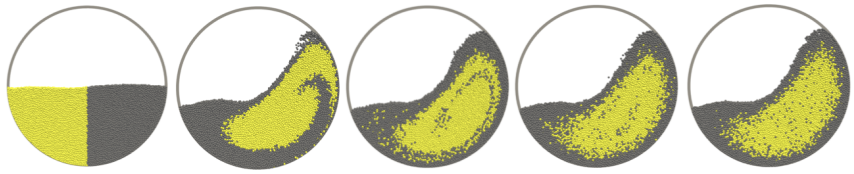

(c) $\rho_o/\rho_b = 3$

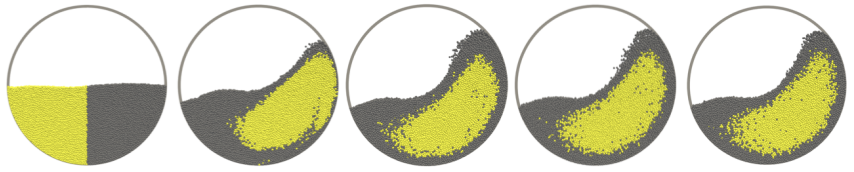

(d) $\rho_o/\rho_b = 4$

Figure 5. Temporal evolutions of mixing patterns for different values of particle density ratio as a function of rotation number N

4. Particle velocity field and free surface

The averaged particle velocity fields in drums of different values of particle density ratio are illustrated in Fig. 6. The velocity vectors are projected on the secant slope. The secant line is defined by joining the uppermost point of the free surface to its lowermost point, as shown in Fig. 2(b). Positive values correspond to particles flowing downward under the effect of the gravity whereas

negative values correspond to upward motion of the particles. From the velocity field, we clearly distinguish the active layer (upper) from the passive layer (lower), as shown in Fig. 6(a). We also see the boundary at the interface between the active and passive layers. The largest velocities are located at the center of free surface where particles are cascading down. The particles in passive layer and near drum wall move with velocity which is slightly smaller than ωR. This is due to the fact that spheres can slide on the smooth drum wall.

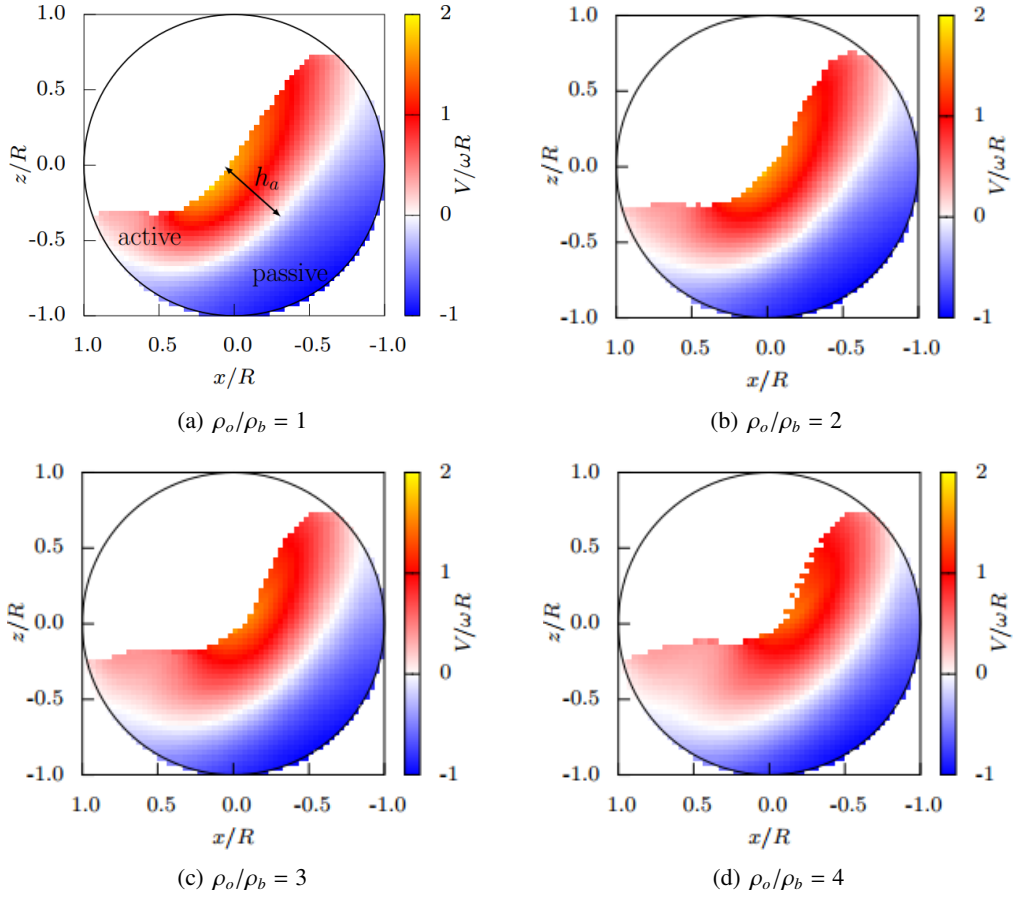

(a) $\rho_o/\rho_b = 1$ (b) $\rho_o/\rho_b = 2$

(c) $\rho_o/\rho_b = 3$ (d) $\rho_o/\rho_b = 4$

Figure 6. Time-averaged particle velocity field in drums of different values of the density ratio. The particle velocity is projected on the secant slope defined by its angle θ_m

The flow thickness h_b is evaluated from the free surface along the line passing by the midpoint of the secant slope and perpendicular to it (see Fig. 2(b)). The active layer thickness h_a is part of h_b, and is defined as the distance from the free surface to the interface between the active and passive layers (see Fig. 6(a)). The active layer thickness h_a is an important parameter for phenomena such as mixing, segregation, and heat transfer in rotating drums.

To characterize the free surface, we define two slope angles: the secant slope θ_m and the tangent slope $\theta_{\max}$ of the steepest descent along the free surface, as shown in Fig. 2(b). The angle $\theta_{\max}$ reflects the kinematics of the free surface flow. The secant slope θ_m represents the average slope of the free surface. The slope ratio $\theta_{\max}/\theta_m$ represents a measure of the curvature of the free surface.

The evolution of slope ratio $\theta_{\max}/\theta_m$ and thickness ratio h_a/h_b as a function of the particle density ratio are shown in Fig. 7. We see that the ratio $h_a/h_b \simeq 0.53$, and $\theta_{\max}/\theta_m \simeq 1.55$ for cascading regime

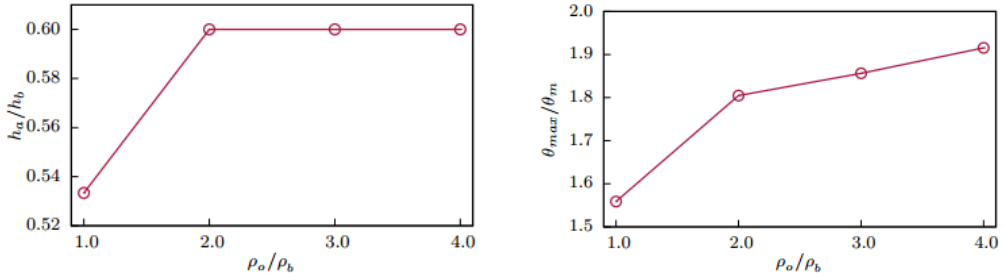

(a) h_a/h_b (b) $\theta_{\max}/\theta_m$

Figure 7. Thickness ratio and slope ratio as a function of the particle density ratio.

of similar particle densities, which is bigger than those of cascading regime composed of octahedral particles proposed in Ref. [21]. This reflects the differences between particle shapes in which spheres can slide on the drum wall while octahedra do not slide. Interestingly, the ratio h_a/h_b increases from 0.53 at $\rho_o/\rho_b = 1$ to 0.6 at $\rho_o/\rho_b = 2$, and then it reaches steady value of 0.6. In contrast, the ratio $\theta_{\max}/\theta_m$ is an increasing function of density ratio. It can reach the value of 1.9 for the largest value of density ratio. Although the mixing index is a decreasing function of the density ratio, the thickness and angle ratios generally increase.

Fig. 8 displays the free surface in drums of different values of the particle density. We see that the secant slope decreases with the density ratio but the maximum slope is an increasing function of the density ratio. This means that the free surface is more curved with larger values of the particle density ratio, as shown in Fig. 7(b). Because the momentum and energy that denser particles transmit to the lighter particles increase with the density ratio, the $\theta_{\max}$ reflecting the kinematic of the free surface also increases.

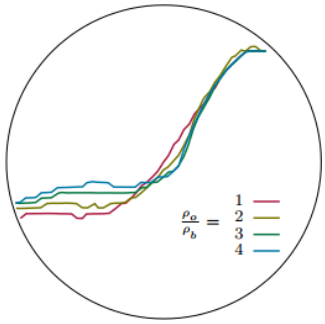

Figure 8. Free surface in rotating drums with different values of the particle density ratio

5. Conclusions

In this study, we used discrete element method to investigate the equi-sized binary mixing of differing density granular material composed of spherical particles in a horizontally rotating cylindrical drum. The analysis was conducted over a range of control parameters for which the flow remains in the cascading regime, characterized by particle flows with a curved free surface. We showed that the powders composed of particles with similar densities mix efficiently, achieving a Lacey mixing index close to 1. However, the mixing index decreases significantly as the particle density ratio increases. This reduction in mixing efficiency arises from the segregation mechanism in which denser particles accumulate in the central region of the drum, while lighter particles migrate toward the drum wall and free surface. We also observed that both the thickness ratio and free-surface angle ratio increase with the particle density ratio. The bigger momentum and energy carried by the denser particles contribute to a steeper free surface slope.

The simulations presented in this study serve as a simplified illustration of the mixing of uranium and plutonium oxide powders during nuclear fuel fabrication. Further work is necessary to evaluate the effect of the particle shape on mixing efficiency in rotating drums, as the actual morphologies of uranium and plutonium oxide aggregates differ significantly from idealized spheres. However, the

spherical-particle approximation allows us to analyze the overall rheological response of granular materials. We are also interested in the effect of both interparticle friction and particle-wall friction on the mixing process, which will be published elsewhere.

References

[1] Parant, P. (2016). Compaction de microsphères poreuses d'oxyde de lanthanides: approche expérimentale et simulations numériques. PhD thesis, Université Grenoble Alpes.

[2] Patrice, B. (1999). Rôle de la distribution des compositions cationiques sur l'aptitude à la dissolution des combustibles MOX: caractérisation de la distribution par diffraction des rayons X sur poudre. PhD thesis, Université Joseph Fourier (Grenoble; 1971-2015).

[3] Orozco, L. F. (2019). Numerical modeling and rheology of crushable granular flows: application to ball mills. PhD thesis, University of Montpellier.

[4] Cayla Arianer, L. (2024). Étude expérimentale et simulation de l'influence des caractéristiques des particules sur le comportement à l'écoulement de poudres modèles. PhD thesis, Université de Technologie de Compiègne.

[5] Tran, T.-D. (2023). Cohesive strength and bonding structure of agglomerates composed of aspherical particles. PhD thesis, University of Montpellier.

[6] La Lumia, F. (2019). Granulation de suspensions concentrées UO2/PuO2 : application à l'élaboration de compacts granulaires denses par pressage et à leu caractérisation structurale post frittage. PhD thesis, Université de Limoges.

[7] Chambon, C. (2017). Densification et homogénéisation U/Pu au cours du frittage de combustibles oxydes mixtes élaborés à partir de poudres UO2, U3O8 et PuO2. PhD thesis, Université de Bordeaux.

[8] La Lumia, F., Ramond, L., Pagnoux, C., Coste, P., Lebreton, F., Sevilla, J.-R., Bernard-Granger, G. (2020). Dense and homogeneous MOX fuel pellets manufactured using the freeze granulation route. *Journal of the American Ceramic Society*, 103(5):3020–3029.

[9] La Lumia, F., Ramond, L., Pagnoux, C., Bernard-Granger, G. (2019). Fabrication of homogenous pellets by freeze granulation of optimized TiO2-Y2O3 suspensions. *Journal of the European Ceramic Society*, 39(6):2168–2178.

[10] Jeon, S.-C., Lee, J.-W., Lee, J.-H., Kang, S.-J., Lee, K.-Y., Cho, Y.-Z., Ahn, D.-H., Song, K.-C. (2015). Fabrication of UO2 Porous Pellets on a Scale of 30 kg-U/Batch at the PRIDE Facility. *Advances in Materials Science and Engineering*, 2015(1):376173.

[11] Picart, S., Parant, P., Caisso, M., Remy, E., Mokhtari, H., Jobelin, I., Bayle, J. P., Martin, C. L., Blanchart, P., Ayral, A., Delahaye, T. (2015). Porous metal oxide microspheres from ion exchange resin. *The European Physical Journal Special Topics*, 224(9):1675–1687.

[12] Vu, D. C. (2023). Quasi-static and dynamic granular flows: scaling behavior, microstructure, and particle shape effects. PhD thesis, University of Montpellier.

[13] Ding, Y. L., Seville, J. P. K., Forster, R., Parker, D. J. (2001). Solids motion in rolling mode rotating drums operated at low to medium rotational speeds. *Chemical Engineering Science*, 56(5):1769–1780.

[14] Aissa, A. A., Duchesne, C., Rodrigue, D. (2012). Transverse mixing of polymer powders in a rotary cylinder part I: Active layer characterization. *Powder Technology*, 219:193–201.

[15] Mellmann, J. (2001). The transverse motion of solids in rotating cylinders—forms of motion and transition behavior. *Powder Technology*, 118(3):251–270.

[16] Alizadeh, E., Dubé, O., Bertrand, F., Chaouki, J. (2013). Characterization of Mixing and Size Segregation in a Rotating Drum by a Particle Tracking Method. *AIChE Journal*, 59(6):1894–1905.

[17] Orozco, L. F., Delenne, J.-Y., Sornay, P., Radjai, F. (2020). Rheology and scaling behavior of cascading granular flows in rotating drums. *Journal of Rheology*, 64(4):915–931.

[18] Govender, N. (2022). A DEM study on the thermal conduction of granular material in a rotating drum using polyhedral particles on GPUs. *Chemical Engineering Science*, 252:117491.

[19] Govender, I. (2016). Granular flows in rotating drums: A rheological perspective. *Minerals Engineering*, 92:168–175.

[20] Yang, R. Y., Yu, A. B., McElroy, L., Bao, J. (2008). Numerical simulation of particle dynamics in different flow regimes in a rotating drum. *Powder Technology*, 188(2):170–177.

[21] Vu, D. C., Amarsid, L., Delenne, J.-Y., Richefeu, V., Radjai, F. (2024). Rheology and scaling behavior of polyhedral particle flows in rotating drums. *Powder Technology*, 434:119338.

[22] Arntz, M. M. H. D., den Otter, W. K., Briels, W. J., Bussmann, P. J. T., Beeftink, H. H., Boom, R. M. (2008). Granular mixing and segregation in a horizontal rotating drum: A simulation study on the impact of rotational speed and fill level. *AIChE Journal*, 54(12):3133–3146.

[23] Xu, Y., Xu, C., Zhou, Z., Du, J., Hu, D. (2010). 2D DEM simulation of particle mixing in rotating drum: A parametric study. *Particuology*, 8(2):141–149.

[24] Soni, R. K., Mohanty, R., Mohanty, S., Mishra, B. K. (2016). Numerical analysis of mixing of particles in drum mixers using DEM. *Advanced Powder Technology*, 27(2):531–540.

[25] Bhateja, A., Sharma, I., Singh, J. K. (2017). Segregation physics of a macroscale granular ratchet. *Physical Review Fluids*, 2(5):052301–.

[26] He, S. Y., Gan, J. Q., Pinson, D., Zhou, Z. Y. (2019). Particle shape-induced radial segregation of binary mixtures in a rotating drum. *Powder Technology*, 341:157–166.

[27] Ji, S., Wang, S., Zhou, Z. (2020). Influence of particle shape on mixing rate in rotating drums based on super-quadric DEM simulations. *Advanced Powder Technology*, 31(8):3540–3550.

[28] Pereira, G. G., Sinnott, M. D., Cleary, P. W., Liffman, K., Metcalfe, G., Šutalo, I. D. (2011). Insights from simulations into mechanisms for density segregation of granular mixtures in rotating cylinders. *Granular Matter*, 13(1):53–74.

[29] Richefeu, V., Combe, G., Villard, P., Delenne, J.-Y., Amarsid, L., Nezamabadi, S., Radjai, F., Vanson, J.-M., Prat, R., Mutabaruka, P. (2025). Rockable.

[30] Richefeu, V., El Youssoufi, M. S., Radjaï, F. (2006). Shear strength properties of wet granular materials. *Physical Review E*, 73(5):051304–.

[31] Herrmann, H. J., Hovi, J.-P., Luding, S. (2013). *Physics of dry granular media*, volume 350. Springer Science & Business Media.

[32] Brilliantov, N. V., Spahn, F., Hertzsch, J.-M., Pöschel, T. (1996). Model for collisions in granular gases. *Physical Review E*, 53(5):5382–5392.

[33] Louge, M. Y. (1994). Computer simulations of rapid granular flows of spheres interacting with a flat, frictional boundary. *Physics of Fluids*, 6(7):2253–2269.

[34] Lacey, P. M. C. (1954). Developments in the theory of particle mixing. *Journal of Applied Chemistry*, 4 (5):257–268.

[35] Jiang, M., Zhao, Y., Liu, G., Zheng, J. (2011). Enhancing mixing of particles by baffles in a rotating drum mixer. *Particuology*, 9(3):270–278.

[36] Yamamoto, M., Ishihara, S., Kano, J. (2016). Evaluation of particle density effect for mixing behavior in a rotating drum mixer by DEM simulation. *Advanced Powder Technology*, 27(3):864–870.

[37] Aissa, A. A., Duchesne, C., Rodrigue, D. (2011). Effect of friction coefficient and density on mixing particles in the rolling regime. *Powder Technology*, 212(2):340–347.

[38] Musha, H., Chandratilleke, G. R., Chan, S. L. I., Bridgwater, J., Yu, A. B. (2013). Effects of size and density differences on mixing of binary mixtures of particles. *AIP Conference Proceedings*, 1542(1): 739–742.

[39] Doucet, J., Hudon, N., Bertrand, F., Chaouki, J. (2008). Modeling of the mixing of monodisperse particles using a stationary DEM-based Markov process. *Computers & Chemical Engineering*, 32(6):1334–1341.

[40] Liu, P. Y., Yang, R. Y., Yu, A. B. (2013). DEM study of the transverse mixing of wet particles in rotating drums. *Chemical Engineering Science*, 86:99–107.

[41] He, S., Gan, J., Pinson, D., Yu, A., Zhou, Z. (2020). A Discrete Element Method Study of Monodisperse Mixing of Ellipsoidal Particles in a Rotating Drum. *Industrial & Engineering Chemistry Research*, 59 (27):12458–12470.